Designing hierarchical porous features of ZSM-5 zeolites via Si/Al ratio and their dynamic behavior in seawater ion complexes

Designing hierarchical porous features of ZSM-5 zeolites via Si/Al ratio and their dynamic behavior in seawater ion complexes

Bo Zhu[a], Cara M. Doherty[b], Xiurong Hu[c], Anita J. Hill[b,d], Linda Zou[e], Y.S. Lin[f], Mikel Duke[a*]

[a] *Institute for Sustainability and Innovation, College of Engineering and Science, Victoria University, Werribee Campus, PO Box 14428, Melbourne, VIC 8001, Australia*

[b]*CSIRO Materials Science and Engineering, Private Bag 10, Clayton South, VIC 3169, Australia*

[c]*Center of Analysis and Measurement, Zhejiang University, Hangzhou, Zhejiang 310058, P. R. China*

[d]*CSIRO Process Science and Engineering, Private Bag 33, Clayton South, VIC 3169, Australia*

[e]*Centre for Water Management & Reuse, University of South Australia, Mawson Lakes Campus, Adelaide, SA 5095, Australia*

[f]*School for Engineering of Matter, Transport and Energy, Arizona State University, Tempe, AZ 85287, USA*

ABSTRACT

MFI-type zeolites were characterized using powder x-ray diffraction (XRD), and positron annihilation lifetime spectroscopy (PALS) to uncover the hierarchical porous

* Corresponding author. Tel: +61 3 9919 7682; fax: +61 3 9919 7696. Email: mikel.duke@vu.edu.au (M. Duke).

properties with Si/Al ratios varying from 30 to >1000 (high silica MFI). Structural dynamics were observed in response to exposure of the zeolites to seawater solutions, mimicking service conditions for use in membrane desalination or other ionic solution applications (e.g. sensors). PALS results indicated MFI channels between 0.27 nm and 0.36 nm. All materials had microporous grain boundaries of 1.1 nm. Mesopores were also detected at approximately 8 nm in size for all materials. However the volume of microporous grain boundaries reduced with increasing alumina as explained by increasing presence of cations. Seawater exposure had a strong and complex effect on all materials. Initially widely variable crystal dimensions were stabilized by seawater exposure. The highest alumina content ZSM-5 (Si/Al = 30) demonstrated net exchange, replacing K^+ from synthesis impurities with Na^+ leading to little overall change in porous features. Higher silica materials, including high silica MFI, demonstrated an overall release of ions, principally Na^+ and K^+, which were liberated mainly from the zeolite channels, yet these materials adsorbed Ca^{2+} in the microporous grain boundaries and Mg^{2+} in the mesoporous grain boundaries. Si/Al = 100 appeared to be a unique ratio, allowing the material to possess the same Na^+ adsorption features (and hydrophilicity) of high alumina materials, but ion interactions resembling high silica materials. MFI-type zeolite is therefore shown to be highly configurable using Si/Al ratio for a wide variety of applications in the presence of ions.

Keywords: MFI Zeolites; Desalination; Ion interactions; PALS; XRD Structure refinement

1. Introduction

Synthetic zeolite materials are highly configurable through their chemistry and have been extensively studied for a variety of applications including catalysis, adsorption, sensing and separation [1-10]. Such materials are potential candidates for water treatment and desalination membranes as they possess the required small pore properties to capture organics and/or reject ions. They offer high tolerance to a variety of realistic feed waters and harsh cleaning methods due to the thermal, chemical and mechanical stability of ceramics [11]. Researchers have explored the use of advanced zeolitic materials to capture micro-pollutants in water which can be highly selective and magnetically separable [1-3]. There has also been some work applying zeolite membranes in the application of desalination [4-10]. Lin et al. [9] conducted a molecular dynamic simulation study on the diffusion of dissolved NaCl through a perfect (single crystal) pure-silica ZK-4 zeolite. Their results showed that the zeolite pore structure is ideally suited for ion rejection due to the size exclusion of hydrated ions. The aperture of the ZK-4 zeolite (diameter 0.42 nm) is significantly smaller than the kinetic sizes of hydrated ions (e.g. Na^+ 0.716 nm, K^+ 0.662 nm, Ca^{2+} 0.824 nm) [12].

More recently, several research groups have developed intact MFI-type zeolites as defect free films by the *in situ* or secondary growth techniques for potential reverse osmosis (RO) desalination [4-8]. Performance testing of MFI type zeolite membranes demonstrated high rejections of even the smallest ions, including Na^+ [4, 7]. For pure silica MFI, a simulation was recently conducted demonstrating that Na^+ can enter the crystal channels, but RO is possible due to the strong resistance by Cl^- to enter the

channels thus inhibiting Na^+ diffusion by maintaining charge balance [13]. Little work however exists on their application in aqueous saline solutions where they can function with significant capacity as ion exchangers, water quality sensors or desalination membranes. The ions in seawater will have strong interactions with the zeolitic structures. To promote and advance the use of zeolites for water treatment applications, a better understanding of the dynamic polycrystalline lattice and grain boundaries of the zeolite membranes as they interact with ions present in these waters is necessary, as this dynamic response will dictate how MFI-type zeolites perform in these applications.

In an ideal molecular sieve zeolite, diffusion should generally occur only through the regular intracrystalline pores within the zeolite cages. In reality, however, the permeation properties will often be modified due to the existence of intercrystalline defect porosity caused by insufficient intergrowth of crystals, thermal removal of the template, or the complete de-watering of the materials [14, 15]. Thermal removal of tetra-propyl ammonium hydroxide (TPAOH), which is commonly used as a structure directing agent for the synthesis of MFI type zeolites, has been extensively studied [16, 17]. The effects of heat treatment on the unit cell dimension of MFI type zeolite crystals have also been reported in literature [15, 18-20]. In addition to the removal of the template and water, the adsorption of guest molecules such as benzene and n-hexane can also cause changes in the structure of zeolites [21-23]. All the observed effects have been attributed to hierarchical properties of zeolites, so facile measurement of these pore spaces and how they change is clearly needed to explain their interaction with guest species.

Material chemistry also plays an important role in explaining interactions. An easily modified feature of MFI-type zeolites is the Si/Al ratio which gives tailored chemical properties for the optimization of sorption uptake and species selectivity [24]. For example, increasing the content of alumina can alter properties such as surface hydrophobicity and surface charge which can have a significant impact on the diffusion of electrolytes [24, 25]. However, little work has been carried out to explore the influence of seawater exposure and ion exchange on the intrinsic lattice dimensions and the intracrystalline and intercrystalline porosity of MFI zeolites. In our previous work, we found that complex solutions of ions sourced from a synthetic seawater solution in turn have complex interactions with low alumina MFI zeolite's inter and intra crystalline spaces [26] that will govern behavior when developed as a membrane for seawater desalination [7]. In this work, we define the complex interactions with one of the most common means of material modification, the ratio of silica to alumina. To tailor zeolite materials for major water quality or treatment applications in the presence of saline waters, a better understanding of structure property relationships at the molecular level is needed. This work presents the effects of interactions between seawater ions and zeolites on the lattice structure, intracrystalline porosity, and intercrystalline porosity of ZSM-5 zeolites.

In order to understand these complex interactions, a reliable method to determine their pore size is needed. N_2 adsorption is one of the most commonly used methods for measuring bulk material pore size but is limited by access of N_2 molecules into the structure. Positron annihilation lifetime spectroscopy (PALS) is an emerging technique for characterization of various materials with pores as small as 1.5 Å in diameter due to

the small size of the positronium probe (Bohr radius 0.53 Å) [26]. Further, positronium can diffuse through the solid phase of the material to reach the pores, so is not reliant on access suiting N_2 molecules to measure porous space.

We prepared ZSM-5 based MFI-type zeolite powders with varied Si/Al ratios to explore the relative uptake of seawater cations by exposing them to synthetic sea salt solutions. Ion interaction experiments were carried out on ZSM-5 zeolites at different exposure times in seawater. Changes in the elemental concentration of major cations in seawater were measured by inductively coupled plasma-optical emission spectroscopy (ICP-OES). PALS was employed to determine the differences in porosity of MFI framework zeolites for the development of a better understanding of the effect of seawater exposure on the molecular structure of zeolites. We utilized X-ray powder diffraction (XRD) to measure the lattice changes associated with seawater exposure.

2. Experimental

2.1. Zeolites preparation

The original MFI zeolite powder samples with different Si/Al ratios were prepared by calcining their suspensions synthesized by a standard hydrothermal process [7] at 525 °C for 6 h with a heating/cooling rate of 1 °C min^{-1}. The suspension used for the high silica MFI (Si/Al > 1000) powder sample was prepared by hydrothermally treating a solution of 43 mL 1M TPAOH (Aldrich), 0.6 g NaOH (Aldrich) and 8.5 g fumed silica (Aldrich, particle size 0.014 μm, surface area 200±25 m^2 g^{-1}) at 180 °C for 8 h.

The suspensions used for ZSM-5 powder samples were prepared by adding a certain amount of $NaAlO_2$ (Aldrich, 0.023 g, 0.116 g and 0.387 g for MFI500 (Si/Al = 500), MFI100 (Si/Al = 100) and MFI30 (Si/Al = 30), respectively) into the above solution and followed by the same hydrothermal treatment process as above. The synthesized hydrothermal suspensions were thoroughly washed with deionized water (DI water) by repeating centrifugation and redispersion in DI water three times prior to the calcination.

2.2. XRD Structure Refinement

XRD measurements were conducted to determine the crystalline structure of the zeolites before and after seawater exposure. Data collection was performed with D/Max-2550pc x-ray powder diffractometer using CuKα radiation (tube operating at 40 kV and 250 mA) with scintillation detector in the range of 3–90 º 2θ with a 0.02º step and a 1 second per step counting time. Variable slits were used. All the structure refinements were performed using the Rietveld method with MDI Jade 9.0 software (Materials Data Inc., USA).

2.3. PALS

PALS experiments were performed using an automated EG&G Ortec fast-fast coincidence system with fast plastic scintillators and a resolution function of 230 ps FWHM. To measure the long lifetimes, the range of the time-to-amplitude-converter (TAC) was extended to 200 ns and the coincidence unit was removed to improve the

count rates. The 30 μCi ^{22}NaCl source was dried onto 2.54 μm thick Mylar film which required a source correction (1.51 ns, 3.37%). The original and seawater exposed zeolite powder samples were degassed at 150°C under vacuum for 16 hours prior to measurement. The positron source was sandwiched between 2 mm of powdered sample and evacuated to 5×10^{-7} Torr. A minimum of five spectra of 4.5 million integrated counts were collected per sample. The spectra were analyzed using LT9 software and were fitted to five components with τ_1 being fixed to 0.125 ns due to para-positron self-annihilation, and τ_2 ~ 0.35–0.45 ns attributed to free positron annihilation. The average pore diameter for τ_3 was calculated using the Tao-Eldrup model assuming infinitely long cylindrical pore shape [27, 28]. The pore sizes for the long lifetimes (τ_4 and τ_5) were calculated using the rectangular Tao-Eldrup (RTE) model based on an infinitely long channel [29].

2.4. Ion adsorption

The ion adsorption experiments were carried out in a shaking water bath at room temperature. For each ion adsorption experiment, 1 g MFI zeolite powder was mixed with 5 mL seawater (3.8 wt.% TDS (total dissolved solids)) (prepared from sea salts, Sigma-Aldrich) in a 50 mL centrifuge tube and shaken for 48 h. A total of 5 samples of each zeolite were prepared and removed at various time intervals up to 48 hours to determine the ion adsorption at that exposure time. After each adsorption experiment, the mixture was centrifuged (RPM 4000, 10 min) immediately to avoid any further interactions. The supernatant was withdrawn from the tube and analyzed for cations by a Shimadzu ICPE-9000 ICP-OES. The seawater exposed zeolite powder was washed

with DI water three times and oven dried at 80 ºC overnight, and then underwent XRD and PALS measurements. Results obtained from ICP-OES analysis are presented as the amount of ion *i* adsorbed per gram zeolite, $C_{z,i}$, (mmol/g) according to:

$$C_{z,i} = (C_{b,i,0} - C_{b,i,t}) \cdot V / m_z \quad (1)$$

where $C_{b,i,0}$ is the concentration of ion *i* in the bulk supernatant solution initially, $C_{b,i,t}$ is the concentration of ion *i* in the bulk supernatant solution at the end of the experiment (*t* = 48 h), both in mmol/L, m_z is the mass of the zeolite added to the solution (1 g) and *V* is the volume of the solution added to the zeolite powder.

3. Results and Discussion

3.1. Materials characterization before seawater ion exposure

3.1.1. XRD Structure Refinement

XRD was used to determine the crystalline structure of zeolites. The X-ray diffraction pattern (Figure 1a) taken at a wavelength of 1.54 Å (CuKα radiation) for the as synthesized MFI30 powder showed a typical MFI type framework [7, 30] (2θ at around 7.9°, 8.8°, 14.7°, 23.0°, 23.9°, and 29.8° for the major peaks ‘101’, ‘200’, ‘301’, ‘501’, ‘303’, and ‘503’, respectively) with randomly oriented crystals. The other original zeolite samples tested had the same MFI fingerprint patterns (Figure S1) to Figure 1a

but showed slight differences in the most intense Bragg peak (101) between the samples (Fig. 1b inset).

3.1.2. PALS

PALS is able to distinguish between the size and number of pores as well as between the intrinsic zeolite channels, the micropores, and the mesopores. The spectra obtained by PALS for the MFI type zeolite samples were best fitted with five lifetime components, where the last three lifetimes, labeled $\tau_{3,}$ τ_4 and τ_5, are converted to pore sizes within the zeolite samples. Figure 2a shows an example of a timing histogram of the original MFI30 sample fitted with three ortho-positronium (o-Ps) lifetime components ($\tau_{3,}$ τ_4 and τ_5), which are used to calculate the mean pore sizes of the samples. Figure 2b (inset) shows the pore size distribution determined using the PAScual fitting program for PALS analysis [31]. PALS is therefore a useful means to observe the hierarchical structure of MFI-type zeolites, with pores of around 0.27 nm, 1.1 nm, and 7.8 nm corresponding to its intracrystalline/intrinsic zeolite channels, intercrystalline micropores and interparticle mesopores respectively. The latter two are considered to be formed from grain boundaries and space made by the vacated template.

Table 1 shows the porosity of the original zeolite samples measured by PALS. All the samples tested feature three pore sizes from the intrinsic pores, micropores, and mesopores, where the relative concentrations (I_3, I_4 and I_5 in Table 1) and sizes of the pores varied with Si/Al ratio. All zeolite samples showed the same size micropores (~1.1 nm), while the three original ZSM-5 samples had the same pore size for their

intrinsic pores (0.27 nm), while high silica MFI was larger (0.36 nm). There were however significant differences in the size of mesopores (7.8 – 16.7 nm varying with the Si/Al ratio), with a clear trend distinguishable in mean mesopore size even though the mesopore size variability within the samples was appreciable.

The intrinsic zeolite micropores at 0.36 nm and the intercrystalline micropores of 1.06 nm of the high silica MFI (Table 1) are in agreement with those previous published [26]. However the 0.36 nm zeolite micropore size is considerably smaller than that previous reported for MFI zeolites (containing no cations from synthesis) by PALS (0.55 nm±0.03 nm) [32], by low pressure N_2 adsorption (0.54 nm) [33] or by crystallography for the 10-member ring openings (0.56 nm) [6, 30]. 0.36 nm measured in this work could be an average of the accessible intracrystalline spaces as the positrons can access both the 0.55 nm pores and the smaller surrounding chambers within the MFI lattice. Another possible explanation for this difference in pore size is due to the fact that the pore space of MFI zeolites may be filled with sodium or potassium ions from zeolite synthesis, thus reducing the accessible pore diameter [26]. The presence of these cations was not taken into account for the determination of the theoretical radius (0.55 nm) of the pure aluminosilicate structure [34, 35]. Given that previously reported PALS results on MFI zeolite films yield a single uniform pore size of 0.55 nm±0.03 nm [32], the latter explanation is most likely. The partial occupancy and replacement behavior of Na^+ with K^+ may be the reason for the measured smaller pore size in the current work. It has been shown in literature [36] that partial replacement of Na^+ ions with K^+ ions reduces the pore aperture in zeolite NaA (molecular sieve Type 4A) from 0.42 nm to 0.3 nm (molecular sieve Type 3A). In the current work, we measured

intrinsic zeolite micropores at 0.36 nm±0.03 nm. The difference between this measured size and the reported (0.55 nm±0.03 nm) is in a reasonable range. Furthermore, the mesopores measured at 13.5 nm by PALS for high silica MFI zeolites (Table 1) are considerably larger than those from the literature [26, 32]. This is likely to be due to the different synthesis conditions performed within different laboratories. The mesopores are attributed to the interparticle pore space; therefore sample treatment would significantly affect the size and number of these pores due to agglomeration and etching effects [37, 38]. Previous studies have shown that various treatments such as NaOH can contribute to mesopore formation [39, 40].

Changes in relative pore fractions were also observed. The I_3 value representing intrinsic intracrystalline pores steadily decreased with decreasing alumina proportion (increasing Si/Al ratio), meanwhile the larger micropores (I_4) steadily increased in proportion. The mesopores (I_5) also increased in number with decreased alumina content, peaking at MFI500 before dropping significantly for high silica MFI zeolites. The change in Si/Al ratio clearly has an effect on porosity, and it is desirable to understand the mechanisms by which the porosity changes and consequently influences transport properties.

It is known from gas transport studies that with increasing alumina content (decreasing Si/Al ratio), the selectivity of MFI-type zeolite membranes decreases due to the increased presence of grain boundaries [24, 41]. For MFI-type membranes with the highest alumina content (Si/Al = 57) however, a return in selectivity of H_2 permeation to SF_6 as compared to high silica MFI has been attributed to the blocking activity of

adsorbed cations which is unique to high alumina zeolites [41]. In examining the PALS data for these zeolites, the reduction in grain boundaries (I_4) and mesopores (I_5) with respect to the intrinsic pores (I_3) as Si/Al ratio decreases may be explained by the increased presence of cations. Similar to the zeolite membranes where cations were considered to affect gas permeation [41], the zeolite powder samples in our work were also washed in deionized water several times after synthesis. Therefore there is a strong attraction for cations to the zeolite driven by the need to balance alumina's charge as it replaces silica in the framework. So either the higher alumina content membranes, or the high silica MFI membranes, can be expected to exhibit the best separation performance based on size exclusion alone. Therefore, the PALS data appear to correlate with selective gas diffusion properties in membranes made of similar materials [41].

3.2. Ion adsorption

Figure 3 shows the adsorption of major cations within the seawater samples when exposed to the zeolite samples with varying Si/Al ratios. The adsorbed amount determined by Equation 1 was estimated from the ICP-OES measured ion concentrations as shown in Figure S2 and summarized after 48 h in Table S1. In these figures, monovalent ions stabilized more rapidly than divalent as observed before in high silica MFI zeolites [26]. It is observed that the zeolites interact with seawater ions during exposure in a complicated manner, not directly correlating with the Si/Al ratio. K^+ (originating from the templating agent, TPAOH) was released for all materials which is to be expected in the Na^+ dominated system [26]. The most significant

observation is that the zeolites with higher alumina content (MFI30 and MFI100) tended to adsorb Na^+, while lower alumina content (MFI500 and high silica MFI) tended to release it. This had the ultimate effect of a material switching from a net adsorption to net release of cations when immersed in seawater solution as alumina content reduced (Fig. 3). The sudden release of Na^+ occurred in tandem with Ca^{2+} uptake. The uptake of Mg^{2+} gradually increased into the zeolite with increasing Si/Al ratio, except for high silica MFI which took up the least Mg^{2+}. The trend in uptake of Mg^{2+} appears to match the proportion of mesopores (I_5), indicating that the largest ion's uptake occurred within the largest pores, which would correlate well with its size, being the largest ion in hydrated form (0.856 nm). It appears that for the lower alumina content zeolites (higher Si/Al ratio), a weaker association with Na^+ allowed its release to occur in preference to the uptake of Ca^{2+}.

The release of Na^+ and K^+ after exposure, by the high Si content zeolites MFI500 and high silica MFI is most likely due to preferential occupation of the surface by the divalent ions Ca^{2+} and Mg^{2+} [26]. The observed release of K^+ and uptake of Na^+, Mg^{2+} and Ca^{2+}, by MFI30 and MFI100, suggested that K^+ exchanged with not only the divalent cations Ca^{2+} and Mg^{2+}, but also the monovalent ion Na^+. As alumina content increased from the Si/Al = 100 to Si/Al = 30, we see selectivity for K^+ increases such that for Si/Al = 30 there appeared to be no net change in the presence of monovalent cations. ZSM-5 with high alumina (Si/Al = 17.1) demonstrated slight selectivity for K^+ over Na^+ [42], but there is little work exploring the high silica MFI zeolites which is known for its excellent membrane performance [24, 41]. For very high alumina content zeolites (Si/Al around unity), it is expected that zeolites are selective for divalent cations

[42]; however, significant selectivity for divalent ions is not observed in the results in Table S1, with Ca^{2+} only being adsorbed in higher silica materials. Exceptions have been observed for MAP-type zeolites when the crystalline structure can specifically accommodate such ions. Also, work specifically on ZSM-5 showed significant preference of Na^{+} over Ca^{2+} [43]. Indeed in our case, MFI intrinsic pores are too small to accommodate divalent cations so their uptake occurred only in the micropore and mesopore (I_4 and I_5) defects.

3.3. Changes in material properties after seawater ion exposure

3.3.1. Changes in unit-cell dimensions

XRD structure refinement was also carried out on the zeolite samples after 48 h seawater exposure to determine changes in the unit-cell dimensions. The seawater exposed zeolite powder samples measured by XRD had the same MFI fingerprint patterns and similar Rietveld plots (Si/Al = 30 example plot shown in Figure S3) to the original MFI30 sample as shown in Figure 1a.

Figure 4 compares the unit-cell dimensions obtained from Rietveld structural refinement for the zeolite powder samples before and after exposure to seawater ions. Prior to exposure to seawater, there was no trend at all in unit cell dimension with Si/Al ratio. However there were changes in the unit-cell parameters of zeolite samples after exposure to seawater ions where the cell dimensions trended towards equilibrium nearly linear relationship with Si/Al ratio. In order to achieve this apparent equilibrium, the

unit cells either contracted or expanded. A slight overall expansion of the zeolite lattice was observed in the seawater exposed MFI30 and MFI500 samples. While the unit-cell dimensions of MFI100 and high silica MFI became slightly smaller after exposure to seawater ions compared to the original sample, indicating that shrinkage occurred in the lattice structure.

The largest change to crystal size of high silica MFI occurred when there was a replacement of Na^+ predominantly present in the original material with K^+ [26]. Therefore the K^+ trend best indicates crystal change for MFI structures. The trend of K^+ release for each Si/Al ratio in Figure 3 correlates well with the initial unit cell dimensions in Figure 4. Smaller initial crystal unit cells (Si/Al = 30 and 500) expanded and released the largest amount of K^+. Meanwhile larger crystal unit cells (Si/Al = 100 and high silica MFI) contracted but released less K^+. Typically, crystals expand in the presence of ions [43], which makes the observation of contraction for Si/Al = 100 and high silica MFI an unusual finding. However crystal contraction has been observed for zeolites when undergoing dehydration [44]. While our material has undergone the opposite treatment, the same study also concluded that the presence of ions is responsible for significant deformation of the native zeolite framework upon dehydration. During synthesis, materials with more K^+ from synthesis impurities (found in TPAOH) contracted more significantly during calcination to remove the template. Upon ‘conditioning’ in a standard solution of ion-rich seawater, the crystals conformed to equilibrium and either contracted or expanded relative to their deformed state from synthesis to achieve this more relaxed structure. So our experimental synthesis technique appears to have not led to uniform initial crystal dimensions as a function of

Si/Al ratio. Although we rinsed the zeolites several times during synthesis prior to calcination, even slight changes in K^+ will have an impact on the crystal size of MFI. Regardless, post-treatment of zeolites in a solution predominantly containing Na^+ appeared to bring uniformity to the crystals.

3.3.2. Changes in porosity measured by PALS

The porosity of the seawater treated ZSM-5 samples was also measured by PALS. Changes in diameter (Fig. 5a) and relative fraction (I_3, I_4 and I_5) (Fig. 5b) of pores after exposure to seawater ions were observed. Overall, the general trend in pore size change was mostly similar with the exception of Si/Al = 30 showing completely opposite behavior to all other materials. The pore size of the zeolite channels (intrinsic pores calculated from τ_3) and micropores (calculated from τ_4) increased slightly for Si/Al = 30, but decreased for all remaining materials, most significantly for the highest silica materials (Si/Al = 500 and high silica MFI). The mesopores (calculated from τ_5) increased in size for all materials except for Si/Al = 30 which showed a decrease in size of mesopores.

The proportion of the three pore domains (Fig. 5b) revealed uniform trends for all materials. The effect of seawater exposure was minor on Si/Al = 30, but slightly increased the presence of I_3 zeolite channels (particularly MFI500 and high silica MFI), and significantly increased the I_5 mesopores. The I_4 micropores were reduced in direct relation to decreasing alumina in the zeolite. There is clearly a complex effect on porous properties due to exposure to seawater ions.

While we have so far discussed changes to the crystal structure as a result of seawater exposure, the dimensional changes in the porous properties far exceed that of the crystal changes, indicating that changes in pore size and volume are more likely due to physical occupancy by the ions. For seawater exposed MFI30, there were almost no changes in the sizes and quantities of the pores, except for the decrease in mesopore size (from 7.8 nm to 5.8 nm). This higher alumina zeolite was found in our previous work to have a weaker negative charge [7], which is attributed to the strong association of the cations which are known to block grain boundaries [24, 41] which seems to align with our finding, suggesting that Na^{+} or even Mg^{2+} filled this pore space due to the strong attraction associated with the need to counterbalance the alumina present in the structure. When high alumina NaA zeolite (Si/Al = 1) was exposed to high concentration of NaCl (0.17M) or seawater solutions, it was shown to undergo a change from a negative to a positive surface charge at neutral pH indicating it's affinity for cations [10].

MFI100 showed little change of the intracrystalline micropore and mesopore sizes upon ion exposure (< 4%), but showed a large decrease in the intercrystalline micropore size (~ 9%). This is due to larger divalent ions filling this space, specifically Mg^{2+} and not Ca^{2+} according to Figure 3, which can fit into these pores (~ 1.1 nm). A much greater uptake of Na^{+} occurred compared to its higher alumina counterpart Si/Al = 30, but the only pores that appeared to fill were the grain boundary micropores (τ_4). The strong increase in mesopore proportion without significant change to pore size indicates the formation of new pores such that Mg^{2+} maybe encouraging particle agglomeration,

hence creating more mesopores. We suspect Mg^{2+} for this activity because its behavior as a function of Si/Al ratio seems to correlate with the ion uptake function in Figure 3. Mg^{2+} is a larger ion than Ca^{2+} when hydrated, so it would naturally prefer the mesoporous space when Ca^{2+} dominates smaller pore spaces. This is indeed apparent because the I_4 micropore (grain boundary) proportion (Fig. 5b) decreases sharply as the material evolves to high silica MFI, correlating with a sudden rise in Ca^{2+} uptake (Fig. 3). This result is in agreement with our previous study on high silica MFI where mesopores were found to widen and increase in number as a function of seawater exposure time as slower moving divalents moved into the structure and brought particles together [26].

For the higher silica materials, Si/Al = 500 and high silica MFI (Si/Al >1000), the trends in pore structure changes on exposure to seawater ions became more uniform. Unlike the higher alumina materials, these materials uniquely exhibited a net release of ions, predominantly Na^{+}. Of all the materials, the higher silica materials exhibited a reduction in τ_3 mean channel size, but slight increase in I_3 intensity of the intrinsic zeolite pores which can be explained by the vacating of ions originally occupying the smaller regions of the channels. However uniquely we see Ca^{2+} adsorb in these materials which appears to correlate with the reduction in size (τ_4) and intensity (I_4) of the micropore grain boundaries (I_4). As for the other materials, Mg^{2+} interacted and potentially assisted the growth of mesopores.

One of the purposes of our work was to uncover features of MFI-type zeolite materials that give scientists more avenues for control, such as the Si/Al ratio. In Noack

et al.'s [24] work, the Si/Al ratio was investigated in detail using membrane permeation to explain material features. They concluded that as the alumina content increases, so too does the contribution of intercrystalline diffusion (micro or mesoporous grain boundaries identified by PALS). Our data confirm this finding in the sense that high silica MFI has the lowest contribution of mesopores which would reduce the diffusion of the larger molecule gases in size selective separations. Our work further confirms their finding that very high alumina content actually leads to defect blocking and higher membrane selectivity since we measured a gradual decline in micropore grain boundaries (Table 1) possibly due to increasing presence of cations as discussed in Section 3.1.2. This increased attraction explained our observation of significant further uptake of Na^+ and Mg^{2+} into the material when exposed to seawater (Fig. 3).

ZSM-5 with a Si/Al ratio of around 100 has showed some unique features in the literature [7, 24]. For example, Duke et al. [7] found that MFI zeolites with a Si/Al ratio of 100 had a 30% increase in flux during seawater desalination as compared to pure water, while other ratios showed a typical decrease in flux after the introduction of seawater. Unlike gas separation where cations simply block diffusion, water transport is tied to the hydrophilicty of the zeolite. Uniquely Na^+ entered Si/Al = 100 in greater abundance than any other material, which would increase the number of water molecules inside the structure, assuming Na^+ is associated with 6 other water molecules in its hydrated state. This ratio is more hydrophilic than other Si/Al ratios due to the presence of more Na^+ residing in the zeolite channels and micropore grain boundaries. This is in direct agreement with work demonstrating that the water to i-propanol selectivity peaked on membranes with approximately the same ratio, Si/Al = 119 [24],

explained using thorough-membrane permeation studies, as being the unique compromise of hydrophilicity and contributions from grain boundaries. Therefore Si/Al =100 appears to be a unique material in pervaporation applications as it favorably permeates water due to its stronger charge to attract water molecules (and associated Na^+, Fig. 3) borne from the higher alumina presence, but possesses a structural behavior that begins to resemble high silica MFI (Fig. 5).

4. Conclusions

Here we have demonstrated that MFI zeolites (high silica MFI and ZSM-5) possess a hierarchical, trimodal porous structure consisting of the intrinsic (0.27 nm for ZSM-5 and 0.36 nm for high silica MFI) and intercrystal (1.1 nm) micropores as well as a mesoporous domain (7.8 – 16.7 nm varying with the Si/Al ratio). This feature lends itself to complex effects in the presence of a range of monovalent and divalent ions but can be explained by ion chemistry and physical size. By comparing ion adsorption within a range of Si/Al ratio MFI-type zeolites against porosity measured by PALS, we were able to describe the unique effects on each pore size related to the individual cations in synthetic seawater. At highest alumina content (Si/Al = 30), the material tended to exchange K^+ for Na^+ exhibiting little net ion uptake. However, decreasing the alumina content led to a range of effects on porous properties and ion interactions. The Si/Al = 100 material featured the largest uptake of Na^+ (~0.2 mmol/g), occupying the micropore grain boundaries which can influence its performance in water diffusion applications. In lower alumina materials (Si/Al = 500 to Si/Al >1000), the zeolites released Na^+ (~0.25 mmol/g for MFI500 and ~0.14 mmol/g for high silica MFI) from

the zeolite channels due to weaker attraction and displayed uptake of divalent cations with higher charge density, namely Ca^{2+}, into grain boundaries. Mg^{2+} appeared to interact with mesopores, potentially causing agglomeration of particles evidenced by the growth in size and volume of mesopores. These key conclusions and other specific effects observed help guide optimal design of zeolitic materials for sensors, sorbents and membranes.

Acknowledgements

The financial support provided by the Australian Research Council (ARC) through a Discovery Project (DP0986192) is gratefully acknowledged. C.M.D. and A.J.H. acknowledge the CSIRO OCE Science Leader Scheme for support.

References

[1] Y. Deng, C. Deng, D. Qi, C. Liu, J. Liu, X. Zhang, D. Zhao, Synthesis of Core/Shell Colloidal Magnetic Zeolite Microspheres for the Immobilization of Trypsin, Advanced Materials, 21 (2009) 1377-1382.

[2] D.J. Doocey, P.N. Sharratt, C.S. Cundy, R.J. Plaisted, Zeolite-Mediated Advanced Oxidation of Model Chlorinated Phenolic Aqueous Waste: Part 2: Solid Phase Catalysis, Process Safety and Environmental Protection, 82 (2004) 359-364.

[3] W. Wang, M. Zhou, Q. Mao, J. Yue, X. Wang, Novel NaY zeolite-supported nanoscale zero-valent iron as an efficient heterogeneous Fenton catalyst, Catalysis Communications, 11 (2010) 937-941.

[4] L.X. Li, J.H. Dong, T.M. Nenoff, R. Lee, Desalination by reverse osmosis using MFI zeolite membranes, Journal of Membrane Science, 243 (2004) 401-404.

[5] L.X. Li, J.H. Dong, T.M. Nenoff, R. Lee, Reverse osmosis of ionic aqueous solutions on a MFI zeolite membrane, Desalination, 170 (2004) 309-316.

[6] L.X. Li, J.H. Dong, T.M. Nenoff, Transport of water and alkali metal ions through MFI zeolite membranes during reverse osmosis, Separation and Purification Technology, 53 (2007) 42-48.

[7] M. Duke, J. O'Brien-Abraham, N. Milne, B. Zhu, Y.S. Lin, J.C. Diniz da Costa, Seawater desalination performance of MFI type membranes made by secondary growth, Separation and Purification Technology, 68 (2009) 343-350.

[8] M. Kazemimoghadam, T. Mohammadi, Synthesis of MFI zeolite membranes for water desalination, Desalination, 206 (2007) 547-553.

[9] J. Lin, S. Murad, A computer simulation study of the separation of aqueous solutions using thin zeolite membranes, Molecular Physics, 99 (2001) 1175-1181.

[10] C.H. Cho, K.Y. Oh, S.K. Kim, J.G. Yeo, P. Sharma, Pervaporative seawater desalination using NaA zeolite membrane: Mechanisms of high water flux and high salt rejection, Journal of Membrane Science, 371 (2011) 226-238.

[11] E.E. McLeary, J.C. Jansen, F. Kapteijn, Zeolite based films, membranes and membrane reactors: Progress and prospects, Microporous and Mesoporous Materials, 90 (2006) 198-220.

[12] S. Murad, K. Oder, J. Lin, Molecular simulation of osmosis, reverse osmosis, and electro-osmosis in aqueous and methanolic electrolyte solutions, Molecular Physics, 95 (1998) 401-408.

[13] Z.E. Hughes, L.A. Carrington, P. Raiteri, J.D. Gale, A Computational Investigation into the Suitability of Purely Siliceous Zeolites as Reverse Osmosis Membranes, The Journal of Physical Chemistry C, 115 (2011) 4063-4075.

[14] M. Noack, P. Kölsch, A. Dittmar, M. Stöhr, G. Georgi, M. Schneider, U. Dingerdissen, A. Feldhoff, J. Caro, Proof of the ISS-concept for LTA and FAU membranes and their characterization by extended gas permeation studies, Microporous and Mesoporous Materials, 102 (2007) 1-20.

[15] M. Noack, M. Schneider, A. Dittmar, G. Georgi, J. Caro, The change of the unit cell dimension of different zeolite types by heating and its influence on supported membrane layers, Microporous and Mesoporous Materials, 117 (2009) 10-21.

[16] X. Lin, J.L. Falconer, R.D. Noble, Parallel Pathways for Transport in ZSM-5 Zeolite Membranes, Chemistry of Materials, 10 (1998) 3716-3723.

[17] U. Illgen, R. Schäfer, M. Noack, P. Kölsch, A. Kühnle, J. Caro, Membrane supported catalytic dehydrogenation of iso-butane using an MFI zeolite membrane reactor, Catalysis Communications, 2 (2001) 339-345.

[18] D.S. Bhange, V. Ramaswamy, Negative thermal expansion in silicalite-1 and zirconium silicalite-1 having MFI structure, Materials Research Bulletin, 41 (2006) 1392-1402.

[19] M. Lassinantti Gualtieri, A.F. Gualtieri, J. Hedlund, The influence of heating rate on template removal in silicalite-1: An in situ HT-XRPD study, Microporous and Mesoporous Materials, 89 (2006) 1-8.

[20] M. Lassinantti Gualtieri, C. Andersson, F. Jareman, J. Hedlund, A.F. Gualtieri, M. Leoni, C. Meneghini, Crack formation in α-alumina supported MFI zeolite membranes

studied by in situ high temperature synchrotron powder diffraction, Journal of Membrane Science, 290 (2007) 95-104.

[21] B.F. Mentzen, F. Lefebvre, Flexibility of the MFI silicalite framework upon benzene adsorption at higher pore-fillings: a study by x-ray powder diffraction, NMR and molecular mechanics, Materials Research Bulletin, 32 (1997) 813-820.

[22] C.J. Gump, R.D. Noble, J.L. Falconer, Separation of Hexane Isomers through Nonzeolite Pores in ZSM-5 Zeolite Membranes, Industrial & Engineering Chemistry Research, 38 (1999) 2775-2781.

[23] H. Morell, K. Angermund, A.R. Lewis, D.H. Brouwer, C.A. Fyfe, H. Gies, Structural Investigation of Silicalite-I Loaded with n-Hexane by X-ray Diffraction, 29Si MAS NMR, and Molecular Modeling, Chemistry of Materials, 14 (2002) 2192-2198.

[24] M. Noack, P. Kölsch, V. Seefeld, P. Toussaint, G. Georgi, J. Caro, Influence of the Si/Al-ratio on the permeation properties of MFI-membranes, Microporous and Mesoporous Materials, 79 (2005) 329-337.

[25] M. Noack, P. Kölsch, A. Dittmar, M. Stöhr, G. Georgi, R. Eckelt, J. Caro, Effect of crystal intergrowth supporting substances (ISS) on the permeation properties of MFI membranes with enhanced Al-content, Microporous and Mesoporous Materials, 97 (2006) 88-96.

[26] B. Zhu, L. Zou, C.M. Doherty, A.J. Hill, Y.S. Lin, X.R. Hu, H.T. Wang, M. Duke, Investigation of the effects of ion and water interaction on structure and chemistry of silicalite MFI type zeolite for its potential use as a seawater desalination membrane, Journal of Materials Chemistry, 20 (2010) 4675 - 4683.

[27] S.J. Tao, Positronium annihilation in molecular substances (liquids and solids), J. Chem. Phys., 56 (1972) 5499-5510.

[28] M. Eldrup, D. Lightbody, J.N. Sherwood, The temperature dependence of positron lifetimes in solid pivalic acid, Chemical Physics, 63 (1981) 51-58.

[29] T.L. Dull, W.E. Frieze, D.W. Gidley, J.N. Sun, A.F. Yee, Determination of Pore Size in Mesoporous Thin Films from the Annihilation Lifetime of Positronium, The Journal of Physical Chemistry B, 105 (2001) 4657-4662.

[30] C. Baerlocher, L.B. McCusker, Database of zeolite structures: http://www.iza-structure.org/databases/

[31] C. Pascual-Izarra, A.W. Dong, S.J. Pas, A.J. Hill, B.J. Boyd, C.J. Drummond, Advanced fitting algorithms for analysing positron annihilation lifetime spectra, Nuclear Instruments and Methods in Physics Research Section A: Accelerators, Spectrometers, Detectors and Associated Equipment, 603 (2009) 456-466.

[32] J. Li, J. Sun, Z. Li, H. Peng, D. Gidley, R. Todd, E., Y. Yan, Evaluation of pore structure in pure silica zeolite MFI low-k thin films using positronium annihilation lifetime spectroscopy, Journal of Physical Chemistry B, 108 (2004) 11689-11692.

[33] C.A. Cooper, Y.S. Lin, Synthesis and characterization of silicalite powders and membranes with micro-meso bimodal pores, Journal of Materials Science, 42 (2007) 320-327.

[34] D.W. Breck, Zeolite Molecular Sieves - Structure, Chemistry, and Use, Wiley, New York, 1974.

[35] A. Cabral-Prieto, I. García-Sosa, J. Jiménez-Becerril, M. Solache-Ríos, S. Bulbulian, Ortho-positronium annihilation in the Na^{+}, Co(II) and Mn(II) A-type zeolites, Microporous and Mesoporous Materials, 69 (2004) 109-118.

[36] V.K. Kaushik, R.P. Vijayalakshmi, N.V. Choudary, S.G.T. Bhat, XPS studies on cation exchanged zeolite A, Microporous and Mesoporous Materials, 51 (2002) 139-144.

[37] J. Pérez-Ramírez, C.H. Christensen, K. Egeblad, C.H. Christensen, J.C. Groen, Hierarchical zeolites: enhanced utilisation of microporous crystals in catalysis by advances in materials design, Chemical Society Reviews, 37 (2008) 2530-2542.

[38] R. Chal, C. Gérardin, M. Bulut, S. van Donk, Overview and Industrial Assessment of Synthesis Strategies towards Zeolites with Mesopores, ChemCatChem, 3 (2011) 67-81.

[39] C. Andersson, J. Hedlund, Effects of exposure to water and ethanol on silicalite-1 membranes, Journal of Membrane Science, 313 (2008) 120-126.

[40] L. Su, L. Liu, J. Zhuang, H. Wang, Y. Li, W. Shen, Y. Xu, X. Bao, Creating Mesopores in ZSM-5 Zeolite by Alkali Treatment: A New Way to Enhance the Catalytic Performance of Methane Dehydroaromatization on Mo/HZSM-5 Catalysts, Catalysis Letters, 91 (2003) 155-167.

[41] M. Noack, G.T.P. Mabande, J. Caro, G. Georgi, W. Schwieger, P. Kölsch, A. Avhale, Influence of Si/Al ratio, pre-treatment and measurement conditions on permeation properties of MFI membranes on metallic and ceramic supports, Microporous and Mesoporous Materials, 82 (2005) 147-157.

[42] M. Kuronen, R. Harjula, J. Jernstrom, M. Vestenius, J. Lehto, Effect of the framework charge density on zeolite ion exchange selectivities, Physical Chemistry Chemical Physics, 2 (2000) 2655-2659.

[43] M. Kuronen, M. Weller, R. Townsend, R. Harjula, Ion exchange selectivity and structural changes in highly aluminous zeolites, Reactive and Functional Polymers, 66 (2006) 1350-1361.

[44] G. Vezzalini, A. Alberti, A. Sani, M. Triscari, The dehydration process in amicite, Microporous and Mesoporous Materials, 31 (1999) 253-262.

Table 1 Comparison of PALS data for the original zeolites.

	Lifetime (ns)			Intensity (%)			Mean pore size (nm)[a]		
Sample	τ_3	τ_4	τ_5	I_3	I_4	I_5	Intrinsic pores (from τ_3)	Micropores (from τ_4)	Mesopores (from τ_5)
MFI30	0.84(0.02)[b]	6.92(0.20)	79.76(3.30)	29.45(1.66)	3.62(0.03)	12.95(0.37)	0.27(0.01)	1.11(0.02)	7.8(0.6)
MFI100	0.83(0.01)	6.11(0.14)	106.29(11.26)	26.65(1.36)	5.95(0.16)	13.18(1.30)	0.27(0.01)	1.05(0.01)	16.7(7.5)
MFI500	0.83(0.03)	6.83(0.10)	95.40(4.26)	20.66(2.13)	9.20(0.31)	18.08(0.64)	0.27(0.01)	1.10(0.01)	11.8(1.5)
High silica MFI	1.08(0.09)	6.26(0.06)	99.89(5.81)	9.41(1.42)	15.45(0.54)	10.52(0.56)	0.36(0.03)	1.06(0.01)	13.5(2.5)

[a] The average pore sizes were calculated from the lifetimes [b] Population standard deviations are in parentheses.

Figure captions:

Fig. 1 XRD pattern of the original MFI30 sample (a) and differences between the most intense Bragg peak (101) for zeolite samples with different Al/Si ratios (b).

Fig. 2 Timing histogram from PALS showing the three o-Ps lifetime components of the original MFI30 sample (a), with the distribution of pore diameter determined by PAScual (b).

Fig. 3 Moles of the major cations in seawater adsorbed after 48 h exposure to zeolites with different Si/Al ratio.

Fig. 4 Unit-cell dimension changes in a-, b- and c-directions after exposure to seawater ions.

Fig. 5 Changes in pore diameters (a) and relative pore fractions (b) in zeolites with different Si/Al ratio after exposure to seawater ions.

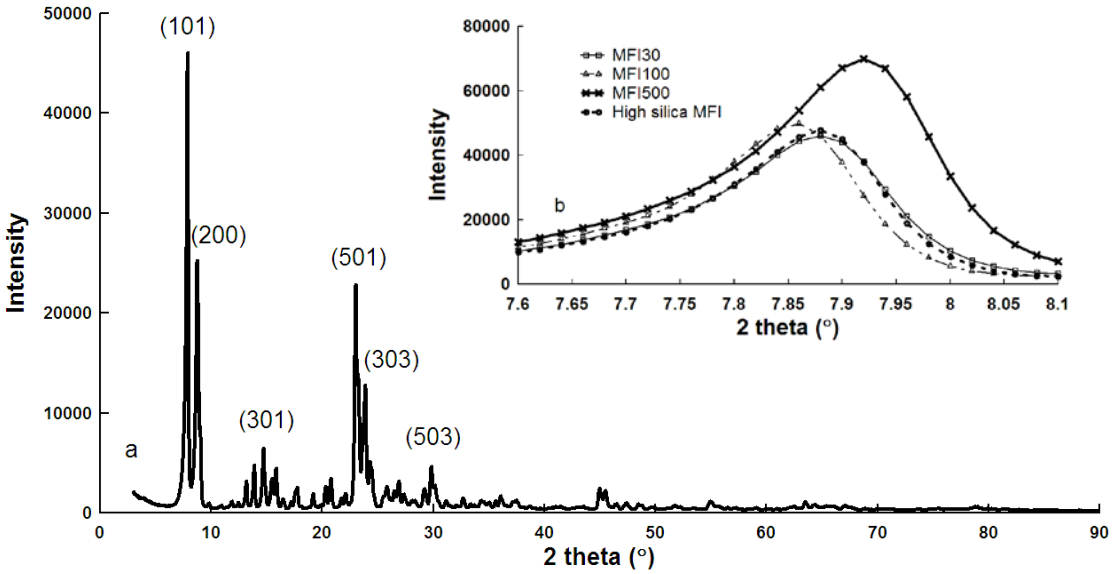
Intensity
2 theta (°)
(101)
(200)
(501)
(303)
(301)
(503)
a
b
MFI30
MFI100
MFI500
High silica MFI

Fig. 1

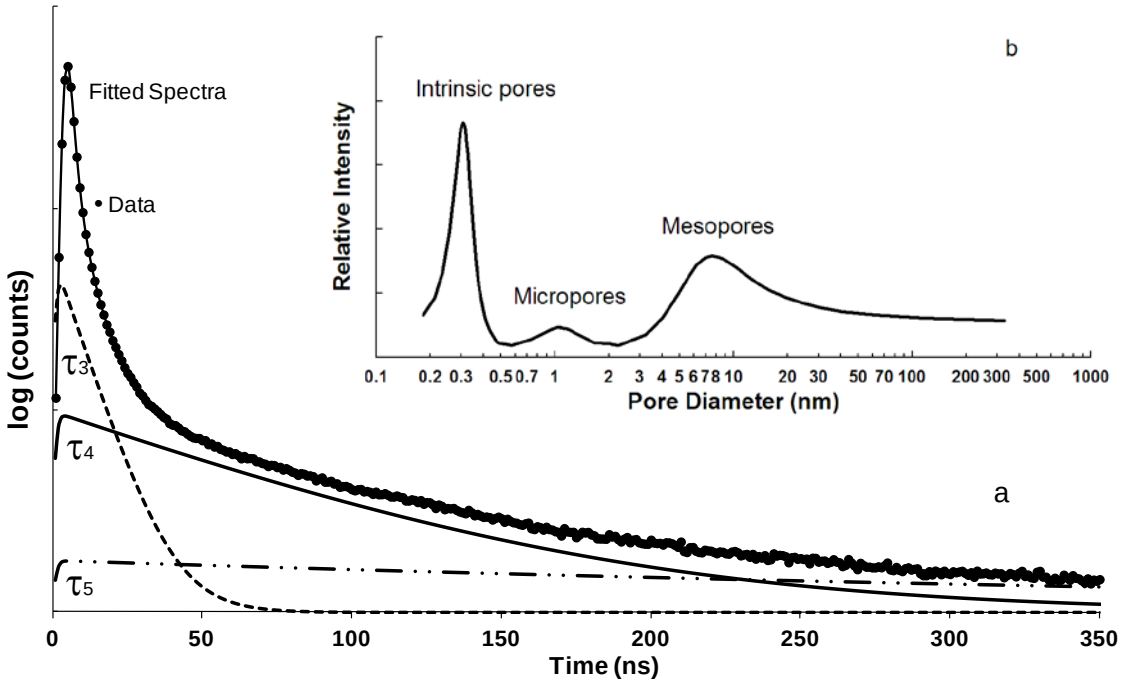
Fitted Spectra
Data
log (counts)
τ3
τ4
τ5
a
b
Intrinsic pores
Micropores
Mesopores
Relative Intensity
0.1 0.2 0.3 0.5 0.7 1 2 3 4 5 6 7 8 10 20 30 50 70 100 200 300 500 1000
Pore Diameter (nm)
0 50 100 150 200 250 300 350
Time (ns)

Fig. 2

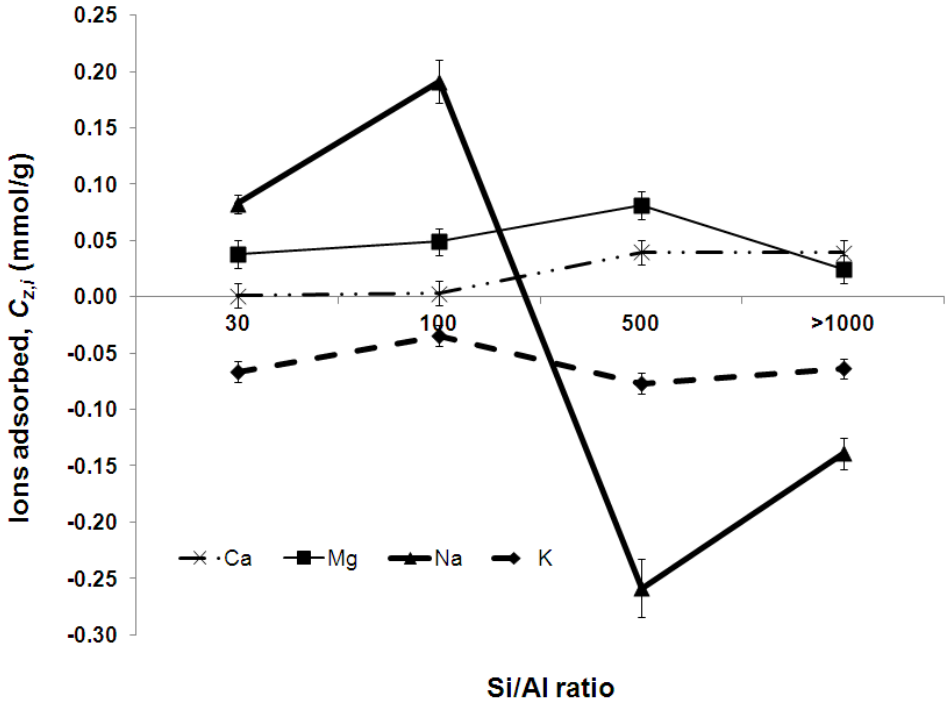
0.25
0.20
0.15
0.10
0.05
0.00
-0.05
-0.10
-0.15
-0.20
-0.25
-0.30
Ions adsorbed, $C_{z,i}$ (mmol/g)
30
100
500
>1000
Ca
Mg
Na
K
Si/Al ratio

Fig. 3

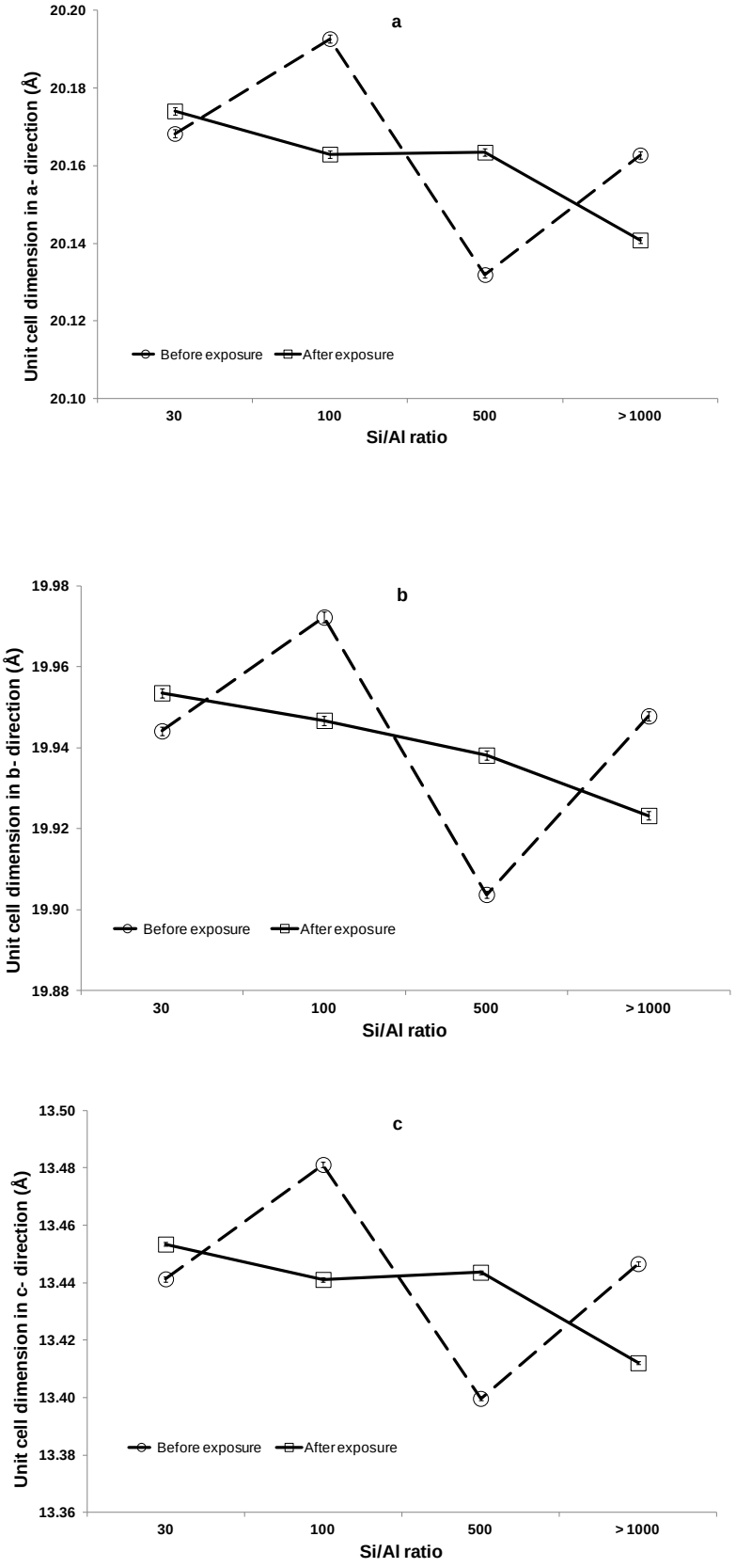
a
Unit cell dimension in a- direction (Å)
20.20
20.18
20.16
20.14
20.12
20.10
Before exposure
After exposure
30
100
500
> 1000
Si/Al ratio
b
Unit cell dimension in b- direction (Å)
19.98
19.96
19.94
19.92
19.90
19.88
Before exposure
After exposure
30
100
500
> 1000
Si/Al ratio
c
Unit cell dimension in c- direction (Å)
13.50
13.48
13.46
13.44
13.42
13.40
13.38
13.36
Before exposure
After exposure
30
100
500
> 1000
Si/Al ratio

Fig. 4

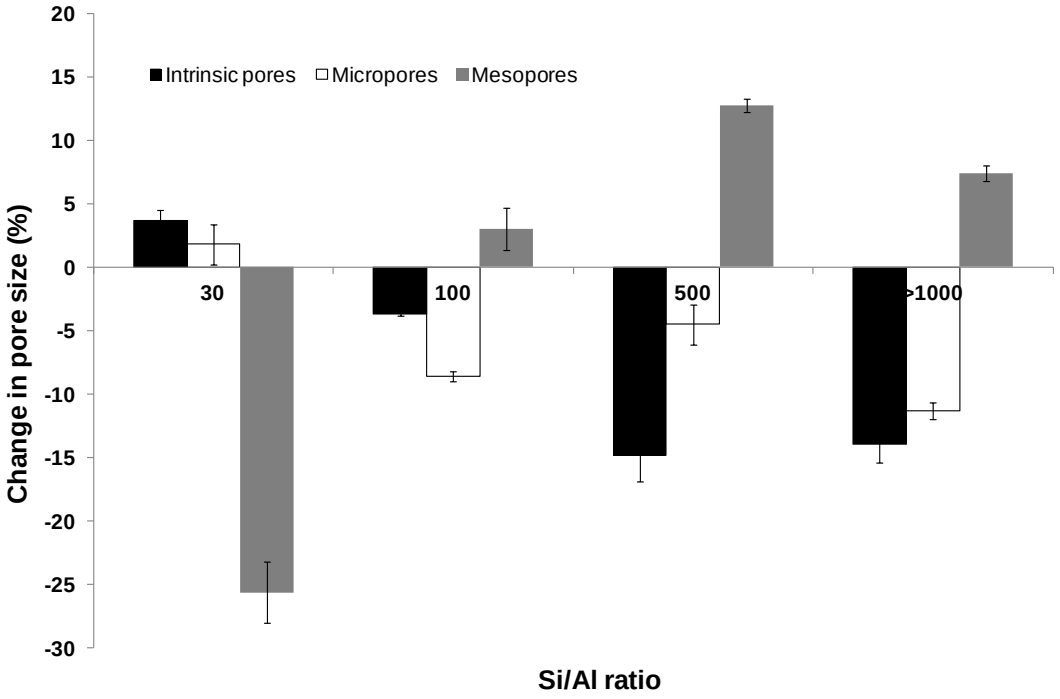
Intrinsic pores
Micropores
Mesopores
Change in pore size (%)
20
15
10
5
0
-5
-10
-15
-20
-25
-30
30
100
500
>1000
Si/Al ratio

(a)

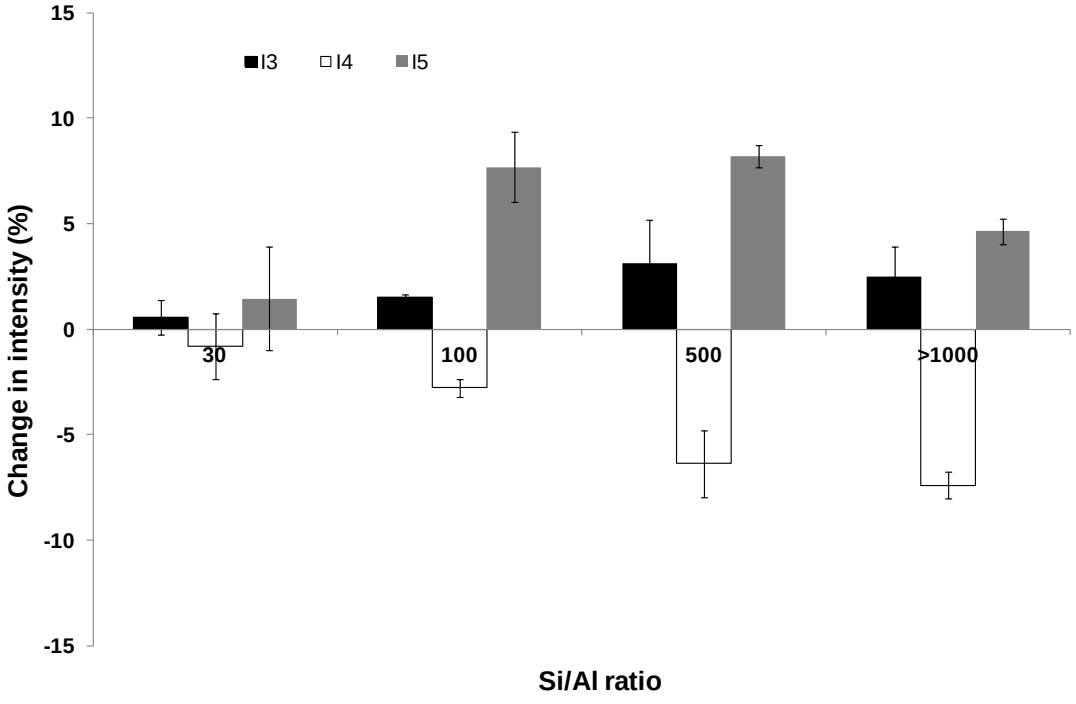
I3
I4
I5
Change in intensity (%)
15
10
5
0
-5
-10
-15
30
100
500
>1000
Si/Al ratio

(b)

Fig. 5.

Supplemental material

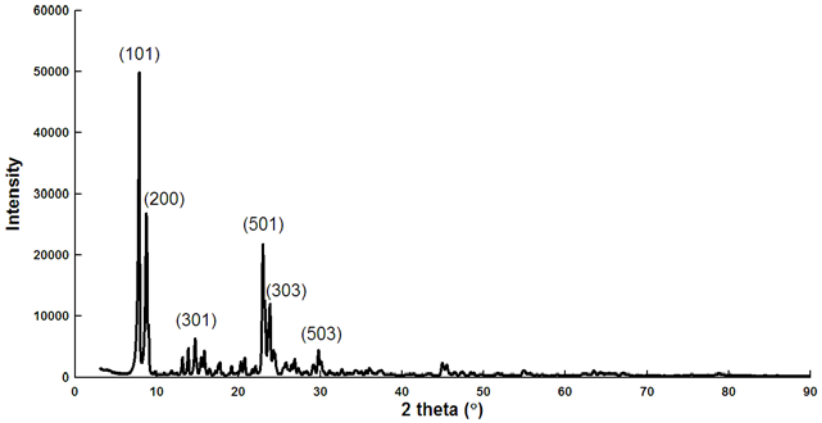

(a) MFI100

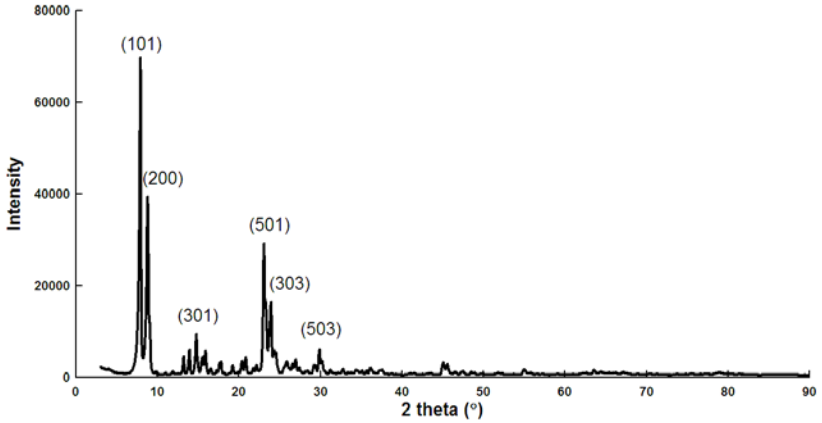

(b) MFI500

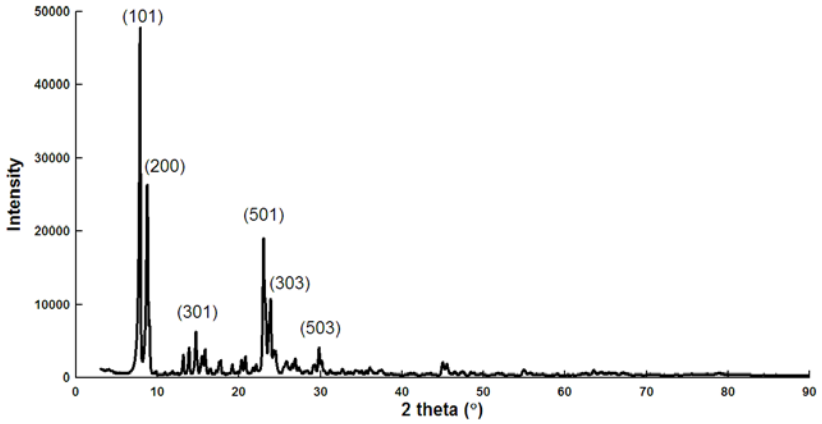

(c) High silica MFI

Fig. S1. XRD pattern of the original zeolite samples.

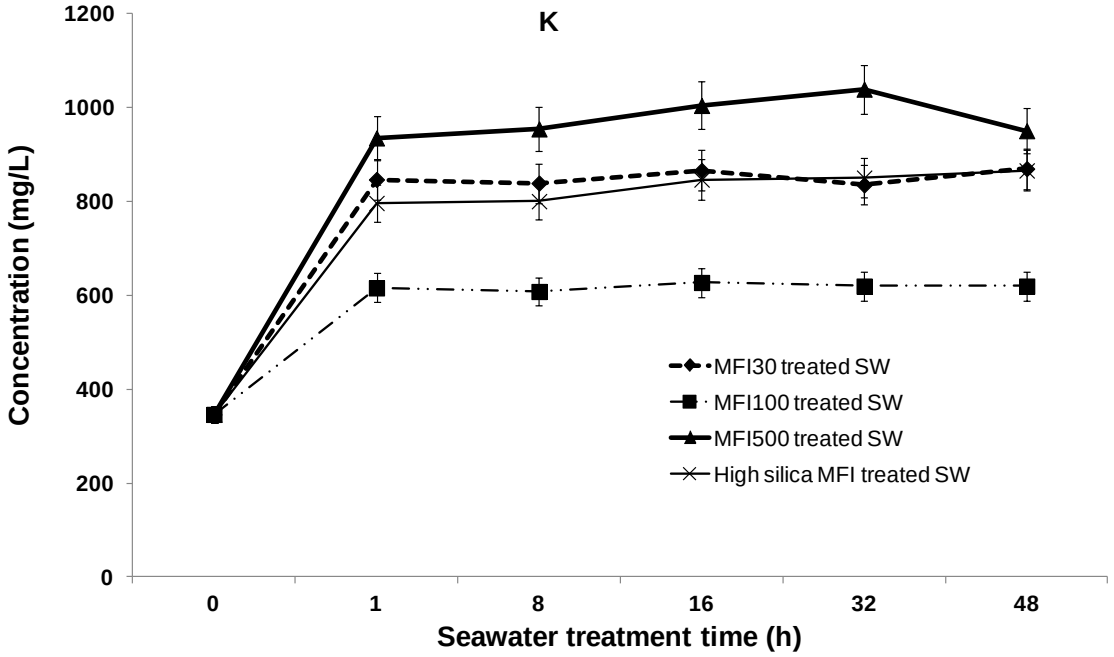
K
Concentration (mg/L)
1200
1000
800
600
400
200
0
0
1
8
16
32
48
Seawater treatment time (h)
MFI30 treated SW
MFI100 treated SW
MFI500 treated SW
High silica MFI treated SW

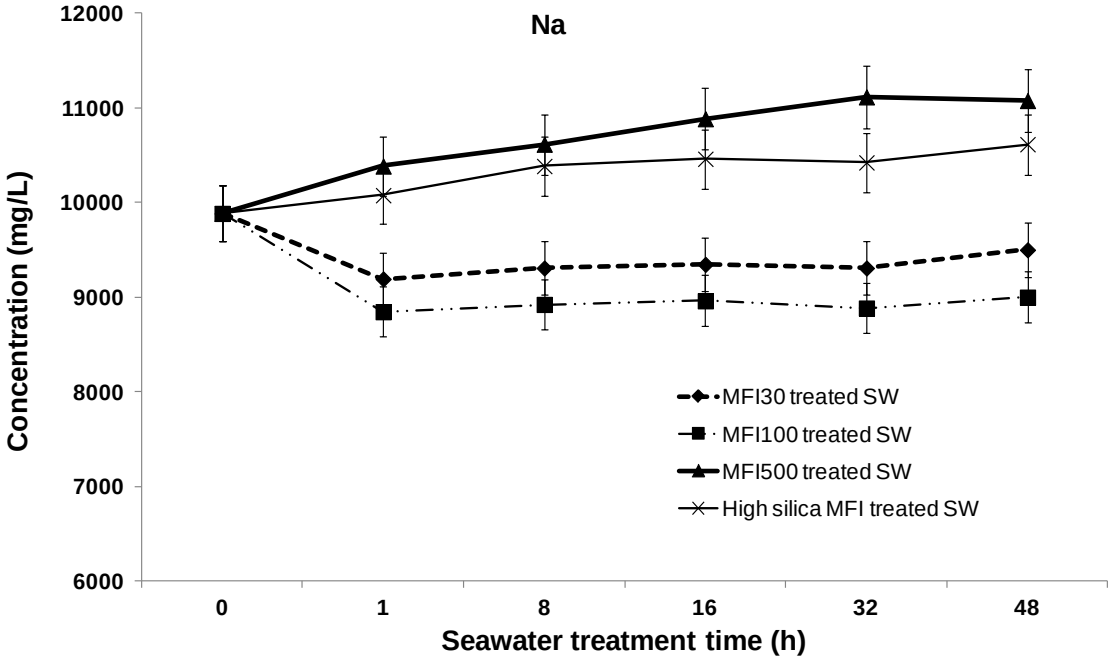
Na
Concentration (mg/L)
12000
11000
10000
9000
8000
7000
6000
0
1
8
16
32
48
Seawater treatment time (h)
MFI30 treated SW
MFI100 treated SW
MFI500 treated SW
High silica MFI treated SW

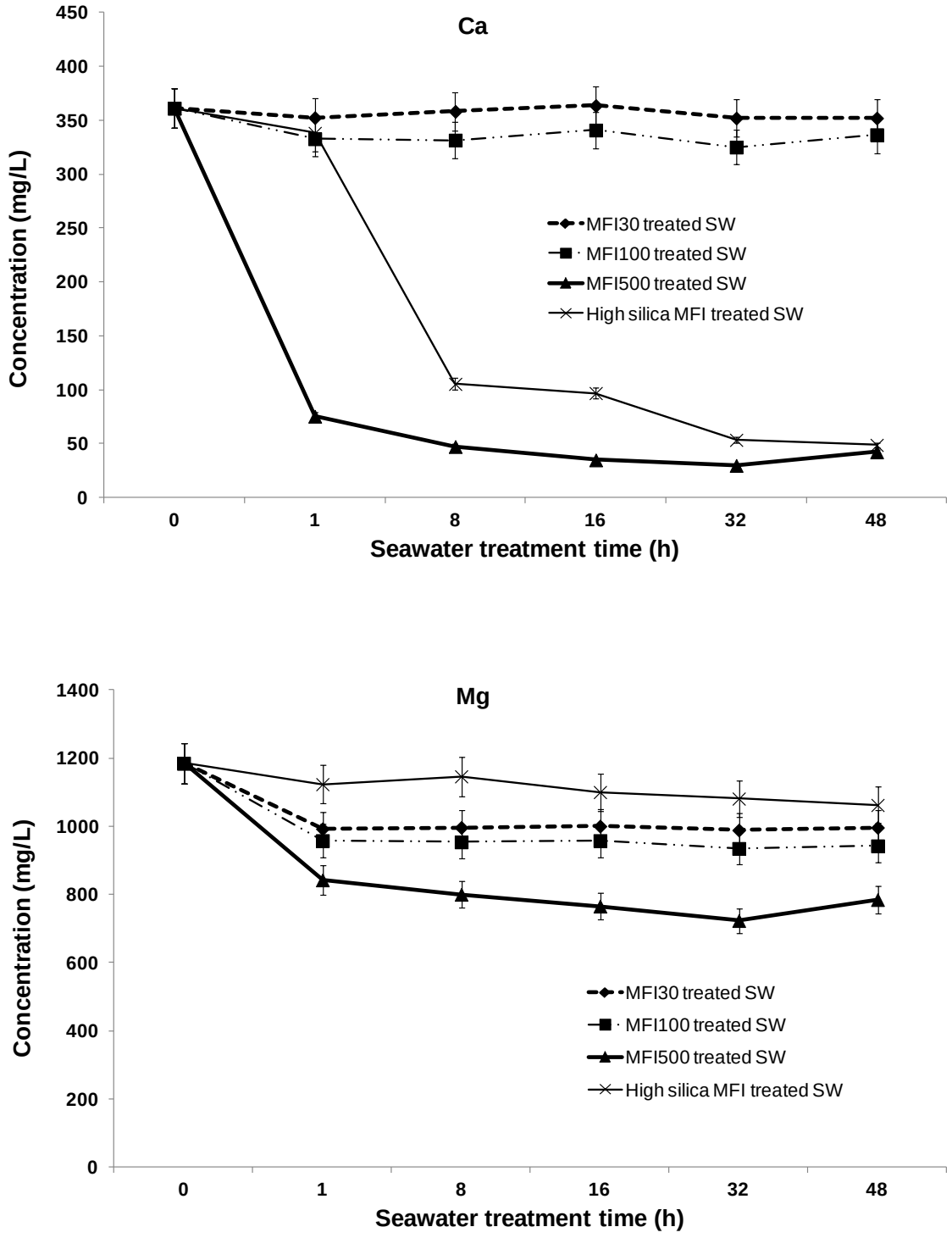

Fig. S2. Variation of concentrations of the major cations in seawater with exposure time. Seawater = 5 mL, zeolite = 1 g. The data for high silica MFI at exposure time 1 h, 8 h, 16 h and 32 h were from our previous work [26].

Table S1 Elemental concentrations of the cations in the untreated seawater (3.8 wt.% TDS) and zeolite treated solutions. Seawater = 5 mL, zeolite = 1 g.

Exposure	Treatment time (h)	Concentration (mg/L)			
		Ca	K	Mg	Na
Unexposed	0	360	350	1180	9880
MFI30	48	351	870	996	9500
MFI100	48	336	619	942	9000
MFI500	48	42	950	785	11070
High silica MFI	48	46	846	1060	10520

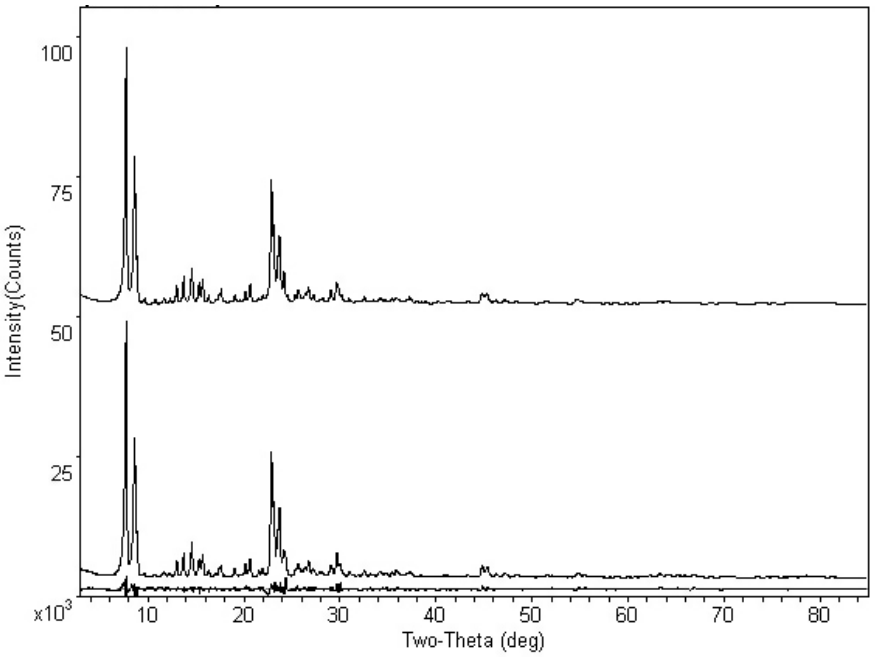

Fig. S3. Rietveld plots for the original MFI30 powder: observed (middle trace), calculated (upper trace) and difference (lower trace) profiles.